INTERNATIONAL JOURNAL FOR NUMERICAL METHODS IN FLUIDS
Int. J. Numer. Meth. Fluids 2006; **51**:1335–1353
Published online 19 January 2006 in Wiley InterScience (www.interscience.wiley.com). DOI: 10.1002/fld.1155

A numerical scheme for strong blast wave driven by explosion

Kaori Kato[1,‡], Takayuki Aoki[1,*,†], Shiro Kubota[2,§] and Masatake Yoshida[2,¶]

[1] *Global Scientific Information and Computing Centre, Tokyo Institute of Technology, 2-12-1 O-okayama, Meguro-ku, Tokyo 152-8550, Japan*
[2] *Research Centre for Explosion Safety, National Institute of Advanced Industrial Science and Technology, 1-1-1 Azuma central 5, Tsukuba-shi, Ibaraki, 305-8565, Japan*

SUMMARY

After the detonation of a solid high explosive, the material has extremely high pressure keeping the solid density and expands rapidly driving strong shock wave. In order to simulate this blast wave, a stable and accurate numerical scheme is required due to large density and pressure changes in time and space. The compressible fluid equations are solved by a fractional step procedure which consists of the advection phase and non-advection phase. The former employs the Rational function CIP scheme in order to preserve monotone signals, and the latter is solved by interpolated differential operator scheme for achieving the accurate calculation. The procedure is categorized into the fractionally stepped semi-Lagrangian. The accuracy of our scheme is confirmed by checking the one-dimensional plane shock tube problem with 10^3 times initial density and pressure jump in comparison with the analytic solution. The Sedov–Taylor blast wave problem is also examined in the two-dimensional cylindrical coordinate in order to check the spherical symmetry and the convergence rates. Two- and three-dimensional simulations for the blast waves from the explosion in the underground magazine are carried out. It is found that the numerical results show quantitatively good agreement with the experimental data. Copyright © 2006 John Wiley & Sons, Ltd.

KEY WORDS: interpolated differential operator scheme; rational function CIP method; blast wave; shock wave; 3-D compressible fluid equations

1. INTRODUCTION

Explosives are very dangerous materials because enormous energy is released at the moment through detonation process. When the detonation process terminated in solid explosives, the pressure reaches tens of thousands times the air and the solid density still remains. The

*Correspondence to: Takayuki Aoki, Global Scientific Information and Computing Centre, Tokyo Institute of Technology, 2-12-1 O-okayama, Meguro-ku, Tokyo 152-8550, Japan.
†E-mail: taoki@gsic.titech.ac.jp
‡E-mail: kaori@sim.gsic.titech.ac.jp
§E-mail: kubota46@aist.go.jp
¶E-mail: m-yoshida@aist.go.jp

Contract/grant sponsor: Grant-in-Aid for Scientific Research from Japan Society for the Promotion of Science; contract/grant number: (B)(2) No. 16360045

Received 17 November 2004
Revised 19 October 2005
Accepted 19 October 2005

detonation product becomes the gas and expands rapidly driving strong shock wave. They are called blast waves. It is noticed that the phenomena is associated with density and pressure changing drastically in time and space. From the view point of safety study, it is very important to estimate damages by blast waves. However, experiments are costly and accompany with many dangers so that numerical simulation is strongly required.

For many years, many sophisticated numerical schemes have been developed in conservative form, for example FCT [1], approximate Riemann solvers [2], TVD [3, 4], ENO [5–8], PPM [9, 10] and others, where successfully good results for shock waves have been achieved and the basic research on blast waves [11–17] have been done. The non-conservative schemes accept more flexible forms for additional terms in the equations, for example chemical reactions, phase changes and so on. However, few non-conservative schemes can give quantitative estimation for wide calculation scales. In the early stage of the blast wave propagation, the large density jump between the detonation product gas and the air makes the numerical simulation difficult. In the neighbourhood of the contact discontinuity, only 0.1% error of the density of the detonation product gas becomes comparable to the air density. In order to study such blast waves, a stable and accurate numerical scheme have to be developed.

In the next section, the governing equations and the numerical scheme is described in the non-conservative form. We apply our simulation code to the one-dimensional plane shock tube problem with 10^3 times the initial density and pressure jump in order to compare with the analytic solution. The one-dimensional spherical explosion into free air is also examined to discuss long-distance shock propagation. The Sedov–Taylor self-similar solution of the blast wave is compared with the numerical result in the two-dimensional cylindrical geometry and the convergence rate and the spherical symmetry are checked. We carry out two- and three-dimensional simulations for the blast waves driven by the explosion in the magazine and we discuss the numerical results in comparison with the experimental data. In the final section, some concluding remarks are given.

2. GOVERNING EQUATIONS

The inviscid compressible fluid equations are employed for the blast waves of the detonation product gas expanding rapidly and the strong shock wave propagating into the air. For the detonation product gas, the JWL equation of state $P_{\mathrm{JWL}}(\rho, e)$ [18] is applied, and the ideal gas equation of state $P_{\mathrm{air}} = (\gamma - 1)\rho e$ is used for the air with the ratio of specific heat $\gamma = 1.4$. In the following equations, the notation ρ is the density, e is the internal energy and $\mathbf{u}$ is the velocity, where u, v and w are the components of $\mathbf{u}$ in the x, y and z direction, respectively. In order to identify the region of the detonation product gas, we introduce a volume fraction α which is taking a value $0 \leqslant \alpha \leqslant 1$. The region occupied by only the detonation product gas is indicated by $\alpha = 1$ and the region for only the air is $\alpha = 0$. The pressure of the mixed region is simply determined by $p = \alpha P_{\mathrm{JWL}} + (1 - \alpha)P_{\mathrm{air}}$. This simple mixture EOS might not be applicable to the phenomena including such chemical reactions as detonation process. We can introduce better mixture model [19, 20] to our scheme, however the choice of the mixture EOS model is not sensitive to the blast wave propagation.

$$\frac{\partial \rho}{\partial t} + (\mathbf{u} \cdot \nabla)\rho = -\rho \nabla \cdot \mathbf{u} \tag{1}$$

$$\frac{\partial \mathbf{u}}{\partial t} + (\mathbf{u}\cdot\nabla)\mathbf{u} = -\frac{1}{\rho}\nabla p \tag{2}$$

$$\frac{\partial e}{\partial t} + (\mathbf{u}\cdot\nabla)e = -\frac{p}{\rho}\nabla\cdot\mathbf{u} \tag{3}$$

$$\frac{\partial \alpha}{\partial t} + (\mathbf{u}\cdot\nabla)\alpha = 0 \tag{4}$$

3. NUMERICAL METHOD

We develop a stable and accurate Eulerian scheme for propagation of strong blast waves. The governing equations (1)–(4) are spilt into the advection phase and the non-advection phase in the same way as the original CIP scheme [21, 22]. The fractional step procedure is introduced for the stability of the scheme. The time-stepping algorithm is shown as follows. The time advance from the nth step to the $(n+1)$th step consists of the following procedure. The dependent variables of the nth time step is integrated to the intermediate step denoted as the symbol $*$ by solving the advection equation. Then the variables are advanced to the $(n+1)$th step by solving the non-advection equation. The above procedure is often categorized into fractionally stepped semi-Lagrangian. Because we need better coupling between the pressure and the velocity for the profile with a steep gradient in the non-advection phase, we adapt a staggered grid configuration for the variable definition points as illustrated in Figure 1. In the following subsection, the detail explanations of each phase are described by the one-dimensional equation for simplicity. We define the symbols $\boldsymbol{f} \equiv (\rho, u, e, \alpha)$ and $\boldsymbol{f_x} \equiv (\rho_x, u_x, e_x, \alpha_x)$ and the subscript x denotes the spatial derivative of the variable. The superscript indicates the time step, for example f^{n+1} indicating the value at the time step $t^{n+1} = t^n + \Delta t$, where the Δt is the time step interval.

3.1. Advection phase

For the advection phase, the equations are shown as follows:

$$\frac{\partial \boldsymbol{f}}{\partial t} + u\frac{\partial}{\partial x}\boldsymbol{f} = 0 \tag{5}$$

$$\frac{\partial \boldsymbol{f_x}}{\partial t} + u\frac{\partial \boldsymbol{f_x}}{\partial x} = -\frac{\partial u}{\partial x}\boldsymbol{f_x} \tag{6}$$

The CIP scheme uses a semi-Lagrangian procedure and the dependent variables after the advection $\boldsymbol{f}^*$ are obtained by shifting the profile by the distance $u\Delta t$. The profile is described by the cubic Hermite interpolation constructed by $\boldsymbol{f}$ and $\boldsymbol{f_x}$. The original CIP scheme makes a little undershoot and overshoot near the contact discontinuity. The undershoot of the profile with 1000 times density jump happens a negative density in the low-density side. In calling the equation of state from a density and an internal energy, the negative density causes the fatal error. In order to avoid it, we use the rational function CIP (RCIP) scheme [23, 24] with monotone preserving for the density and the internal energy. The intermediate density ρ^* and ρ_x^* are obtained by substituting $x - u\Delta t$ into the rational function profile $F(x)$,

$$\rho^* = F(x - u\Delta t) \tag{7}$$

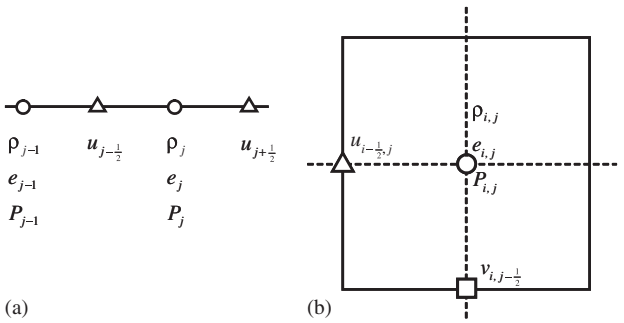

Figure 1. (a) Illustration of the variable definitions on the staggered grid in one-dimensional case; and (b) two-dimensional case.

$$\rho_x^* = \frac{\partial}{\partial x} F(x - u\Delta t) \tag{8}$$

The internal energy e^* and e_x^* are also obtained by the same way as the density. For the velocity u^* and u_x^*, we use the normal cubic Hermite interpolation used in the original CIP, since the monotonicity of the profile is not required.

3.2. Non-advection phase

Near the explosion source, the density changes drastically from the solid to almost vacuum one, and the flow becomes very unstable. The sound waves should be stably calculated with high accuracy. We replace the finite difference method used in the original CIP scheme to the interpolated differential operator (IDO) scheme [25]. We derive the equations for non-advection phase as follows:

$$\frac{\partial \boldsymbol{f}}{\partial t} = \left(-\rho u_x, -\frac{p_x + q_x}{\rho}, -\frac{p+q}{\rho} u_x \right) \tag{9}$$

$$\frac{\partial \boldsymbol{f_x}}{\partial t} = \frac{\partial}{\partial x} \left(-\rho u_x, -\frac{p_x + q_x}{\rho}, -\frac{p+q}{\rho} u_x \right) \tag{10}$$

For the time integration, three-stage Runge–Kutta method [26] is used and the time integration of $\boldsymbol{f}$ and $\boldsymbol{f_x}$ from the intermediate step to the $(n+1)$th step are shown as follows:

$$\boldsymbol{f}^{*1} = \boldsymbol{f}^* + \tfrac{2}{3}\Delta t \boldsymbol{f}_t^*, \quad \boldsymbol{f}_x^{*1} = \boldsymbol{f}_x^* + \tfrac{2}{3}\Delta t \boldsymbol{f}_{xt}^* \tag{11}$$

$$\boldsymbol{f}^{*2} = \boldsymbol{f}^* + \tfrac{2}{3}\Delta t \boldsymbol{f}_t^{*1}, \quad \boldsymbol{f}_x^{*2} = \boldsymbol{f}_x^* + \tfrac{2}{3}\Delta t \boldsymbol{f}_{xt}^{*1} \tag{12}$$

$$\boldsymbol{f}^{n+1} = \boldsymbol{f}^* + \frac{\Delta t}{8}(2\boldsymbol{f}^* + 3\boldsymbol{f}_t^{*1} + 3\boldsymbol{f}_t^{*2}), \quad \boldsymbol{f}_x^{n+1} = \boldsymbol{f}_x^* + \frac{\Delta t}{8}(2\boldsymbol{f}^* + 3\boldsymbol{f}_{xt}^{*1} + 3\boldsymbol{f}_{xt}^{*2}) \tag{13}$$

The scalar variables ρ, e, p are defined at the grid point i (at the position x_i). The velocity u is defined at the grid point $i + 1/2$ (at the position $x_i + \frac{1}{2}\Delta x$ and $\Delta x = x_{i+1} - x_i$). The time derivatives $\boldsymbol{f_t}$ and $\boldsymbol{f_{xt}}$ can be described by

$$\rho_{t,i} = -\rho_i u_{x,i} \tag{14}$$

$$u_{t,i+(1/2)} = -\frac{p_{x,i+(1/2)} + q_{x,i+(1/2)}}{\rho_{i+(1/2)}} \tag{15}$$

$$e_{t,i} = -\frac{p_i + q_i}{\rho_i} u_{x,i} \tag{16}$$

$$\rho_{xt,i} = -\rho_{x,i} u_{x,i} - \rho_i u_{xx,i} \tag{17}$$

$$u_{xt,i+(1/2)} = -\frac{p_{xx,i+(1/2)} + q_{xx,i+(1/2)}}{\rho_{i+(1/2)}} + \frac{p_{x,i+(1/2)} + q_{x,i+(1/2)}}{\rho_{i+(1/2)}} \frac{\rho_{x,i+(1/2)}}{\rho_{i+(1/2)}} \tag{18}$$

$$e_{xt,i} = -\frac{p_{x,i} + q_{x,i}}{\rho_i} u_{x,i} - \frac{p_i + q_i}{\rho_i} u_{xx,i} + \frac{p_i + q_i}{\rho_i} \frac{\rho_{x,i}}{\rho_i} u_{x,i} \tag{19}$$

where q stands for von Neumann–Richtmyer's artificial viscosity [27] shown in the following form:

$$q = \begin{cases} C_L \left(\dfrac{\gamma + 1}{2} \rho \Delta u^2 - \rho C_s \Delta u \right), & \Delta u < 0 \\ 0, & \Delta u > 0 \end{cases} \tag{20}$$

where $\Delta u = u_{i+(1/2)} - u_{i-(1/2)}$ is negative for the compression region, C_s is the sound speed and C_L is the coefficient of artificial viscosity. The spatial profile of $\boldsymbol{f}$ between grids is approximated by the cubic Hermite interpolation again. For $\rho_{i+(1/2)}$ and $\rho_{x,i+(1/2)}$ required in (15) and (18), the density profile is constructed by the function $F(x)$ between x_i and x_{i+1}

$$F(x) = a(x - x_i)^3 + b(x - x_i)^2 + \rho_{x,i}(x - x_i) + \rho_i \tag{21}$$

$$F_x(x) = 3a(x - x_i)^2 + 2b(x - x_i) + \rho_{x,i} \tag{22}$$

$$a = \frac{\rho_{x,i} + \rho_{x,i+1}}{\Delta x^2} + \frac{2(\rho_i - \rho_{i+1})}{\Delta x^3} \tag{23}$$

$$b = \frac{3(\rho_{i+1} - \rho_i)}{\Delta x^2} - \frac{2\rho_{x,i} + \rho_{x,i+1}}{\Delta x} \tag{24}$$

We can obtain the values for $\rho_{i+(1/2)}$ and $\rho_{x,i+(1/2)}$ by substituting $x = x_i + (\Delta x/2)$ into $F(x)$,

$$\rho_{i+(1/2)} = F\left(x_i + \frac{\Delta x}{2}\right) = a\left(\frac{\Delta x}{2}\right)^3 + b\left(\frac{\Delta x}{2}\right)^2 + \rho_{x,i}\left(\frac{\Delta x}{2}\right) + \rho_i \tag{25}$$

$$\rho_{x,i+(1/2)} = F_x\left(x_i + \frac{\Delta x}{2}\right) = 3a\left(\frac{\Delta x}{2}\right)^2 + 2b\left(\frac{\Delta x}{2}\right) + \rho_{x,i} \tag{26}$$

In order to interpolate the velocity derivatives $u_{x,i}$ and $u_{xx,i}$ required in (14) and (17), the function $G(x)$ between $x_{i-(1/2)}$ and $x_{i+(1/2)}$ is similarly constructed,

$$G(x) = c(x - x_{i-(1/2)})^3 + d(x - x_{i-(1/2)})^2 + u_{x,i-(1/2)}(x - x_{i-(1/2)}) + u_{i-(1/2)} \tag{27}$$

$$G_x(x) = 3c(x - x_{i-(1/2)})^2 + 2d(x - x_{i-(1/2)}) + u_{x,i-(1/2)} \tag{28}$$

$$c = \frac{u_{x,i-(1/2)} + u_{x,i+(1/2)}}{\Delta x^2} + \frac{2(u_{i-(1/2)} - u_{i+(1/2)})}{\Delta x^3} \tag{29}$$

$$d = \frac{3(u_{i+(1/2)} - u_{i-(1/2)})}{\Delta x^2} - \frac{2u_{x,i-(1/2)} + u_{x,i+(1/2)}}{\Delta x} \tag{30}$$

By substituting $x = x_i$ into $G(x)$, we obtain

$$u_{x,i} = G_x(x_i) = 3c\left(\frac{\Delta x}{2}\right)^2 + 2d\left(\frac{\Delta x}{2}\right) + u_{x,i-(1/2)} \tag{31}$$

$$u_{xx,i} = G_{xx}(x_i) = 6c\left(\frac{\Delta x}{2}\right) + 2d \tag{32}$$

The time integration of non-advection term by three-stage Runge–Kutta method is performed by substituting (14)–(19) into (11) and (13).

3.3. Extension of the scheme to multi-dimensional case

It is a simple procedure to extend the scheme to multi-dimensional case. The multi-dimensional procedure of the CIP scheme of the advection phase is shown in Reference [28], where the TYPE-C interpolation employs the dependent variables f, f_x, f_y and f_{xy} in two-dimensional case and f, f_x, f_y, f_z, f_{xy}, f_{yz}, f_{zx} and f_{xyz} in three-dimensional case. The multi-dimensional interpolation was done by repetitive use of the one-dimensional interpolation. Also in the non-advection phase, the interpolation function is constructed by the same usage of the dependent variable. For example, when we obtain the higher derivative f_{xxy}, we construct the function $F_y(x)$ with f_y and f_{xy} instead of ρ and ρ_x in the x direction in Equations (20)–(23), and take second differentiation to have $f_{xxy} = (\partial^2/\partial x^2)F_y(x)$. For the derivative f_{xyy}, the function $F_x(x)$ is constructed with f_x and f_{xy} in the y direction. By introducing f_{xy} in two-dimensional case and f_{xy}, f_{xz}, f_{yz} and f_{xyz} in three-dimensional case, the multi-dimensional interpolation procedure is closed self-consistently.

3.4. Accuracy of fractional method

In the propagation of blast waves, the accuracy of numerical scheme is of great importance. We adapt the fractional step procedure and the equation is split into the advection and the non-advection phase. The accuracy of the CIP scheme in the advection phase has third-order both in time and space [29]. The IDO scheme used in the non-advection phase also has third-order accuracy in time and space. We are afraid that the fractional time step procedure reduces the time accuracy to first order. The accuracy of the numerical result depends on which Δt or Δx. The time step Δt is determined by CFL condition in our calculation and small enough, so that Δx is dominant for the accuracy of the numerical result. By using the fractional step procedure, although the time accuracy reduces to first order, the numerical result of our scheme has third-order accuracy in space.

4. EXAMINATION OF THE SCHEME FOR STRONG SHOCK WAVES DRIVEN BY HIGH-DENSE AND HIGH-PRESSURE GAS EXPANSION

First, the accuracy of the scheme is confirmed by the one-dimensional plane shock tube problem with thousands times density difference. Next, in order to examine the scheme, we

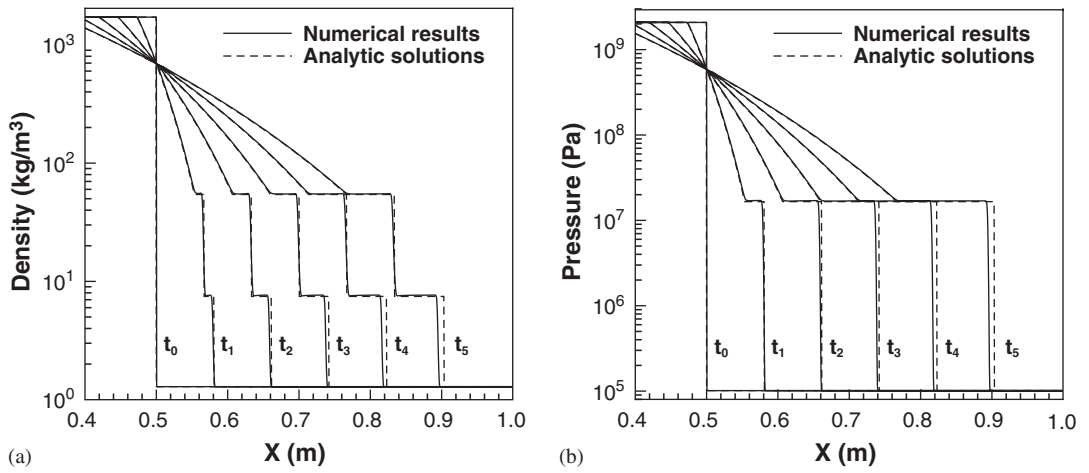

Figure 2. Numerical results of shock tube (solid lines) in comparison with analytic solutions (dashed lines) at $t_0 = 0\,\mu s$, $t_1 = 20\,\mu s$, $t_2 = 40\,\mu s$, $t_3 = 60\,\mu s$, $t_4 = 80\,\mu s$ and $t_5 = 100\,\mu s$: (a) density profiles; and (b) pressure profiles.

apply it to the long-distance propagation of a spherical shock driven by the local energy source.

4.1. Extremely strong shock wave in one-dimensional planer coordinate system

The shock tube problem is one of the most fundamental problems for all the schemes solving shock wave propagation. In the left-hand side region ($0\,m \leqslant x \leqslant 0.5\,m$), a high density of $1630.0\,kg/m^3$ and a high pressure of $2.085 \times 10^9\,Pa$ are set and the standard air of the density $1.225\,kg/m^3$ and the pressure $1.013 \times 10^5\,Pa$ fills the region of the right-hand side ($0.5\,m < x < 1\,m$). The ideal gas equation of state is used with the ratio of specific heat $\gamma = 1.4$. The total grid number $N_x = 2000$ is assigned for the region ($0\,m \leqslant x \leqslant 1\,m$), and the code is run with the parameters of the CFL number of 0.1 and the artificial viscosity coefficient C_L of 2.0.

The comparisons between the numerical results and the analytic solutions for the density and the pressure profiles at the time of $0, 20, 40, 60, 80$ and $100\,ms$ are shown in Figure 2. The solid lines show the numerical results and the dashed lines show the analytic solutions.

In the density profiles, no overshoots and undershoots appear in the vicinity of the contact discontinuity from $\rho = 52.5(51.3)$ to $7.3(7.0)\,kg/m^3$, where the numbers inside the parenthesis indicate the analytic solutions. At the shock wave, the density jump holds six times ahead of the shock of the theoretical value $(\gamma + 1)/(\gamma - 1)$. In the pressure profiles, the jump at the shock wave reaches 166.8(161.9) times ahead of the shock pressure. Although the shock speed of $3.92(4.03)\,m/s$ is slightly small, it is understood that the numerical solutions shows quite good agreement with the analytic solutions in the severe case of the shock tube problem.

4.2. Free explosion into the air in one-dimensional spherical coordinate system

The explosion with the spherical shock propagation into the free air driven by a local energy release is called free explosion, which is a typical benchmark test of one-dimensional blast

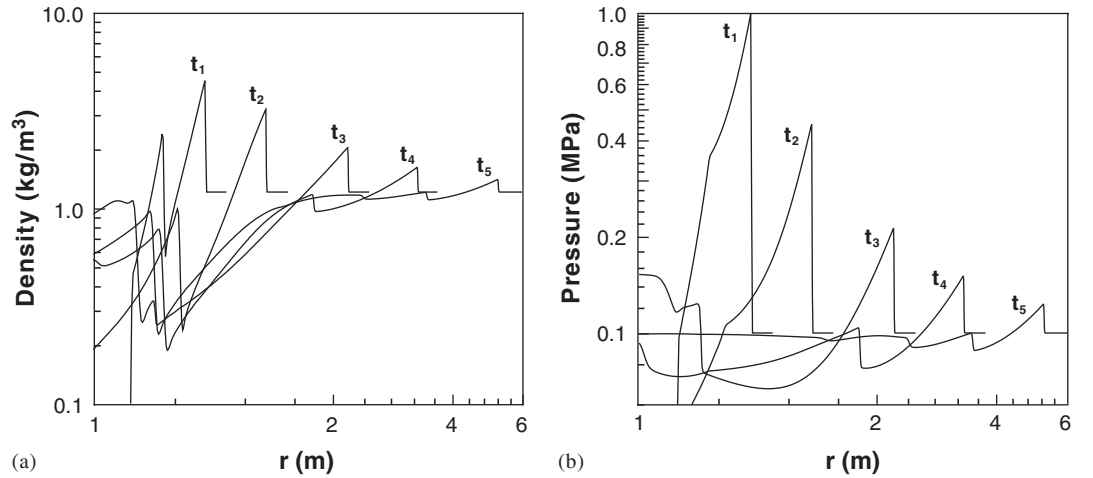

Figure 3. Spherical shock propagation of the free explosion of 1 kg TNT at $t_1 = 0.5$ ms, $t_2 = 1.0$ ms, $t_3 = 2.5$ ms, $t_4 = 5.0$ ms and $t_5 = 10.0$ ms: (a) density profiles; and (b) pressure profiles.

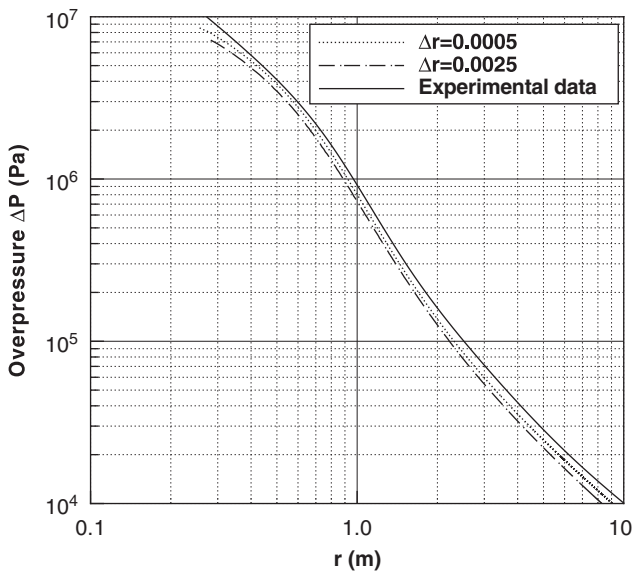

Figure 4. Peak overpressure in the air as function of the shock radius (dashed line and dash–doted line) in comparison with the experimental data (solid line).

wave propagation. Initially, a 1 kg trinitrotoluene (TNT) of the state after the detonation is located in the standard air as the energy source. In the TNT region within the radius 0.0527 m, the density of 1630.0 kg/m^3, the internal energy of 4.29×10^6 J/kg and the pressure of 8.15×10^9 Pa are set and the outside air has the same condition as the previous section. The JWL equation of state is applied to the TNT gas region. The code is run with the parameters of the CFL number of 0.1 and the artificial viscosity coefficient C_L of 2.0. The density and

the pressure profiles of the numerical results with the uniform mesh $\Delta r = 0.0005\,\mathrm{m}$ at the time of $0.5, 1.0, 2.5, 5.0$ and $10.0\,\mathrm{ms}$ are shown in Figure 3. The secondary shock waves are generated by the closer of the central void due to the rarefaction wave. In Figure 3(b), the secondary shock appears clearly at the time $t = 5$ and $10\,\mathrm{ms}$.

We define the overpressure $\Delta P = p - p_0$, where p_0 is the undisturbed air pressure of $1.013 \times 10^5\,\mathrm{Pa}$. The peak of the overpressure as a function of the shock radius r_{shock} is shown in Figure 4. The solid line indicates Baker's experimental result [30]. We execute two cases of the numerical simulation for the region of $0 \leqslant r \leqslant 10\,\mathrm{m}$ with the grid number of $N_r = 10\,000$ and $20\,000$. The dashed line and the dash–doted line represent the numerical results with $\Delta r = 0.0025\,\mathrm{m}$ $(N_r = 10\,000)$ and $\Delta r = 0.0005\,\mathrm{m}$ $(N_r = 20\,000)$, respectively.

The numerical simulation can trace the experimental result very well over the wide region of the spherical shock propagation. It is also found that the simulation with finer mesh size gives better result.

5. EXAMINATION OF THE SEDOV–TAYLOR BLAST WAVE IN TWO-DIMENSIONAL CYLINDRICAL COORDINATE

The Sedov–Taylor blast wave solution [31–34] is well known to be a good benchmark test to study a strong explosion problem. The self-similar solution in the spherical geometry describes the shock wave driven by a point source explosion into a uniform medium. In order to check the convergence rate and the spherical symmetry of our calculation results, we examine this problem in the two-dimensional cylindrical (r, z) geometry. We set the analytic profile of the Sedov–Taylor solution of the time $t_0 = 0.96\,\mu\mathrm{s}$ for the point source of $3.2\,\mathrm{MJ}$ which is

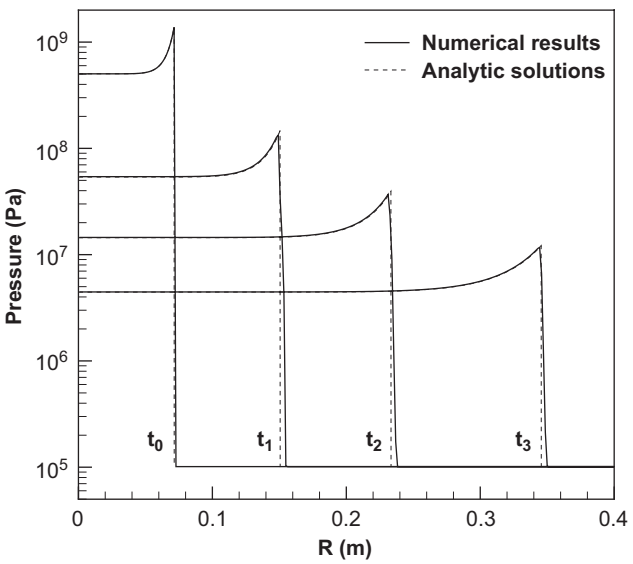

Figure 5. The pressure profiles (solid lines) in comparison with analytic solutions (dashed lines) at the time t_0, $t_1 = t_0 + 5\,\mu\mathrm{s}$, $t_2 = t_0 + 15\,\mu\mathrm{s}$ and $t_3 = t_0 + 40\,\mu\mathrm{s}$.

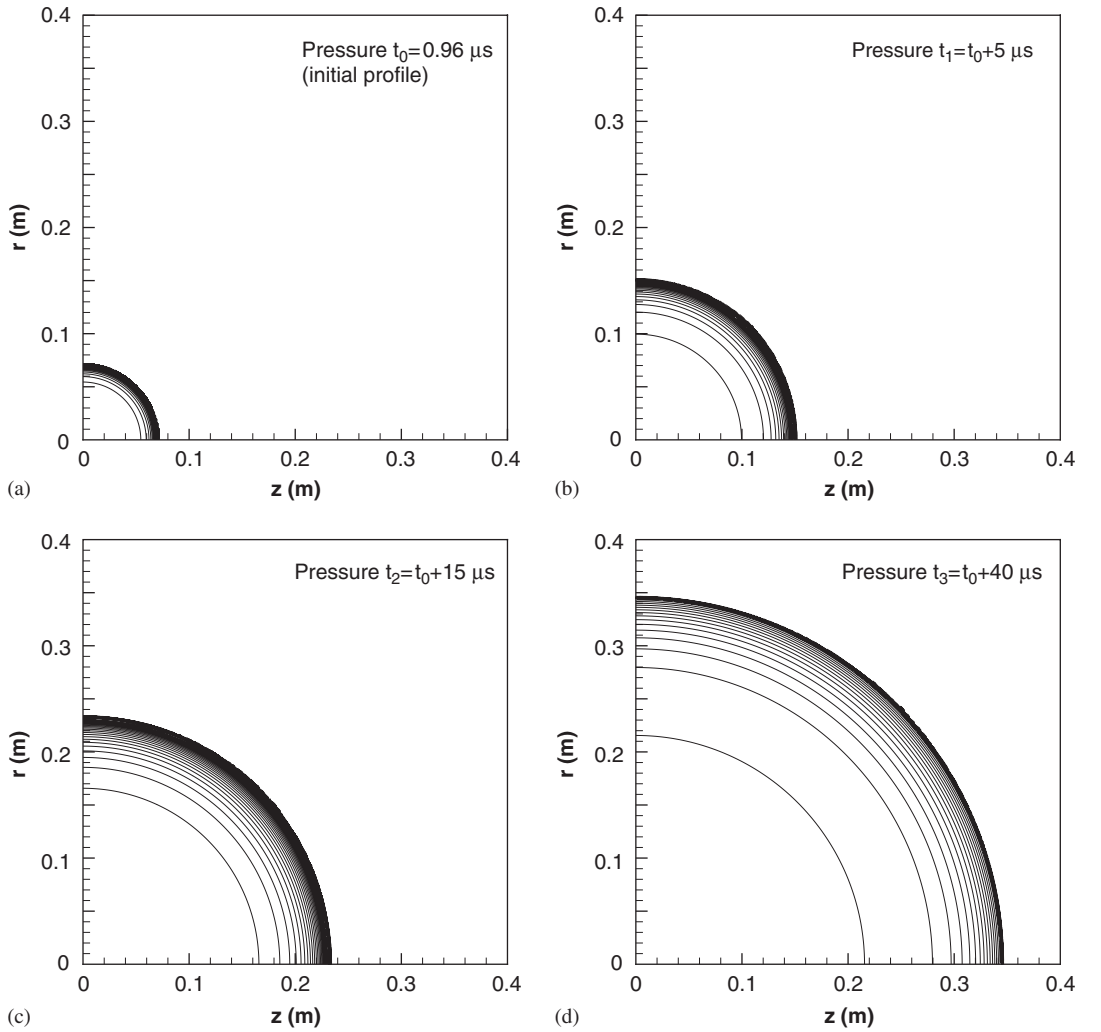

Figure 6. The pressure contours of the Sedov–Taylor blast wave problem at the time t_0, $t_1 = t_0 + 5\,\mu s$, $t_2 = t_0 + 15\,\mu s$ and $t_3 = t_0 + 40\,\mu s$.

corresponding to the 1 kg TNT, as the initial profile of the density, the pressure and the velocity u and v. The expanding process is calculated by our code for the area of $0 \leqslant r \leqslant 0.4$ m and $0 \leqslant z \leqslant 0.4$ m. The time-evolving analytical solution is set for the central region $R \leqslant 0.01$ m to avoid the singularity, where $R = \sqrt{r^2 + z^2}$ is the distance from the centre. The code is run with the CFL number of 0.2 and the artificial viscosity coefficient C_L of 2.0. The comparisons between the numerical results and the analytic solutions for the pressure profiles on the line $r = z$ at the time t_0, $t_0 + 5\,\mu s$, $t_0 + 15\,\mu s$ and $t_0 + 40\,\mu s$ are shown in Figure 5. The solid lines indicate the numerical results with 400×400 mesh, the dashed lines are the analytic solutions. The pressure contours of the numerical results are shown in Figure 6. It is found

Table I. Errors from the analytic solution for the Sedov problem.

Mesh (Test)	Error
100×100 (Test 0)	$E_0 = 2.37 \times 10^{-1}$
200×200 (Test 1)	$E_1 = 3.08 \times 10^{-2}$
400×400 (Test 2)	$E_2 = 3.92 \times 10^{-3}$

that the numerical results keep the spherical symmetry and they show good agreement with the analytic solutions.

The calculations of 100×100 and 200×200 mesh are also carried out to estimate the convergence rate measured by the $E = (1/N)\Sigma(|P_C - P_A|/P_A)$, where N is the grid number inside the shock wave and the subscripts C and A mean the calculated and analytical pressures, respectively. The errors from the analytic solution of E_0, E_1 and E_2 are shown in Table I and we have the convergency $E_0/E_1 = 7.7$ and $E_1/E_2 = 7.8$. It is confirmed that the scheme has the third-order accuracy $7.8–2^3$ in space. We also check the spherical symmetry for the 100×100 calculation of $t_0 + 40\,\mu s$. The deviation from the spherical profile is less than 0.1% for the shock position and the other iso-surfaces of the pressure. The spherical symmetry of our calculation is well kept on the orthogonal mesh.

6. MULTI-DIMENSIONAL SIMULATION FOR THE BLAST WAVE PROPAGATION AROUND THE MAGAZINE

Explosives are often kept in the magazine-like storage space built under the ground or the slope of the mountains. It is necessary to estimate the damage of human and buildings for the explosion accident in such a storage space. The detonation gas produced by the explosion propagates in the outlet direction multiply reflecting at the magazine inner wall and finally erupts into the air. The shock waves expand spherically, however the erupted gas has faster velocity than the sound velocity and continues to drive the shock waves. The shock strength depends on the propagation direction, and they are diffracted at the outlet edge or the outside buildings, so that multi-dimensional blast wave simulations are needed. Many experimental studies have also been done for a mock of the underground magazine. We follow the experiments by two- and three-dimensional numerical simulations and compare with the experimental data.

6.1. Two-dimensional simulation for the blast wave propagation around the magazine driven by the 0.1 kg pentolite explosion in cylindrical coordinate

The simulation for the blast wave driven by the 0.1 kg pentolite is performed in the two-dimensional cylindrical coordinate where the z-axis is chosen to be the axial direction of the magazine and the radial direction is denoted as r. The schematic of the system is shown in Figure 7(a). A mock of the underground magazine is a hollow tube whose one side is closed as shown in Figure 7(b).

In the initial condition, the gas of the state just after the detonation is set as the energy source in the region of $-0.95\,m \leqslant z \leqslant -0.0908\,m$ and $0.0\,m \leqslant r \leqslant 0.022\,m$. The gas has the

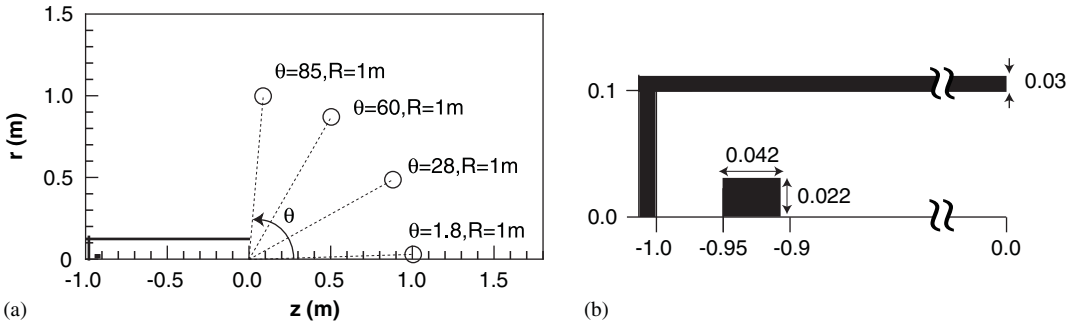

Figure 7. Computational domain of two-dimensional cylindrical coordinate: (a) a schematic of magazine with measurement points; and (b) details inside a magazine with 0.1 kg pentolite.

density of 1640.0 kg/m^3, internal energy of 5.225×10^6 J/kg and the pressure of 7.67×10^9 Pa, and employs the JWL equation of state. The undisturbed air has the same density and pressure as that of Section 4. The total grid number of $N_r \times N_z = 600 \times 1120$ is assigned to the area of 1.5 m $\times$ 2.8 m and the mesh size is $\Delta x = \Delta z = 0.0025$ m. The magazine of 0.1 m in radius, 1.0 m in length and 0.11 m in thickness is implemented as the rigid wall boundary in the simulation. The code is run with the CFL number of 0.1 and the artificial viscosity coefficient C_L of 2.0.

The expansion of the detonation product gas in the confined space makes the flow turbulent due to multiple interactions with the magazine wall. In the numerical result, the front of the blast wave reaches the outlet at the time 0.39 ms. The contour plots of the density and pressure profiles at the time of 0.45, 1.12 and 2.31 ms are shown in Figure 8. When the detonation gas erupts from the magazine outlet, the front velocity of the blast wave rapidly decreases due to switching to three-dimensional expansion from one dimension. The shock wave in the air is detached from the detonation product gas and starts to propagate spherically as shown in Figure 8(a1) and (b1). The spherically expanding front of the primary shock wave into the air is described well in all the contour plots. The contact discontinuity between the air and the detonation product gas becomes clear in the density profiles of the later time Figure 8(a2) and (a3). The Kelvin–Helmholtz instability drives the turbulence of the detonation product gas. At the time of 1.12 ms, the low-density void appears due to the rapid expansion in Figure 8(a2), and the secondary shock waves are generated in closing void region. The complex shock waves are found in the middle of the pressure profile in Figure 8(b3). The axial eruption of the detonation product gas keeps faster velocity than the sound velocity of the air and pushes the shock wave ahead. The shock front is swelled in the axial direction as shown in Figure 8(a2).

In the experiment [35], the pressure histories were measured on the ground at several points keeping 1 m distance from the outlet with various angles of 1.8, 28, 60 and 85° to the z-axis. The overpressure histories at each point are shown in Figure 9. The dashed lines show the numerical results and we compare with the experimental data indicated by the solid lines. In each Figure, the sudden jumps of the overpressure mean the arrival of the primary shock wave. Many small peaks after the jump come from the secondary shock waves. The arrival time of the primary shock is slightly delayed, however the peak and the decay time of the overpressure are in good agreement with the experimental data.

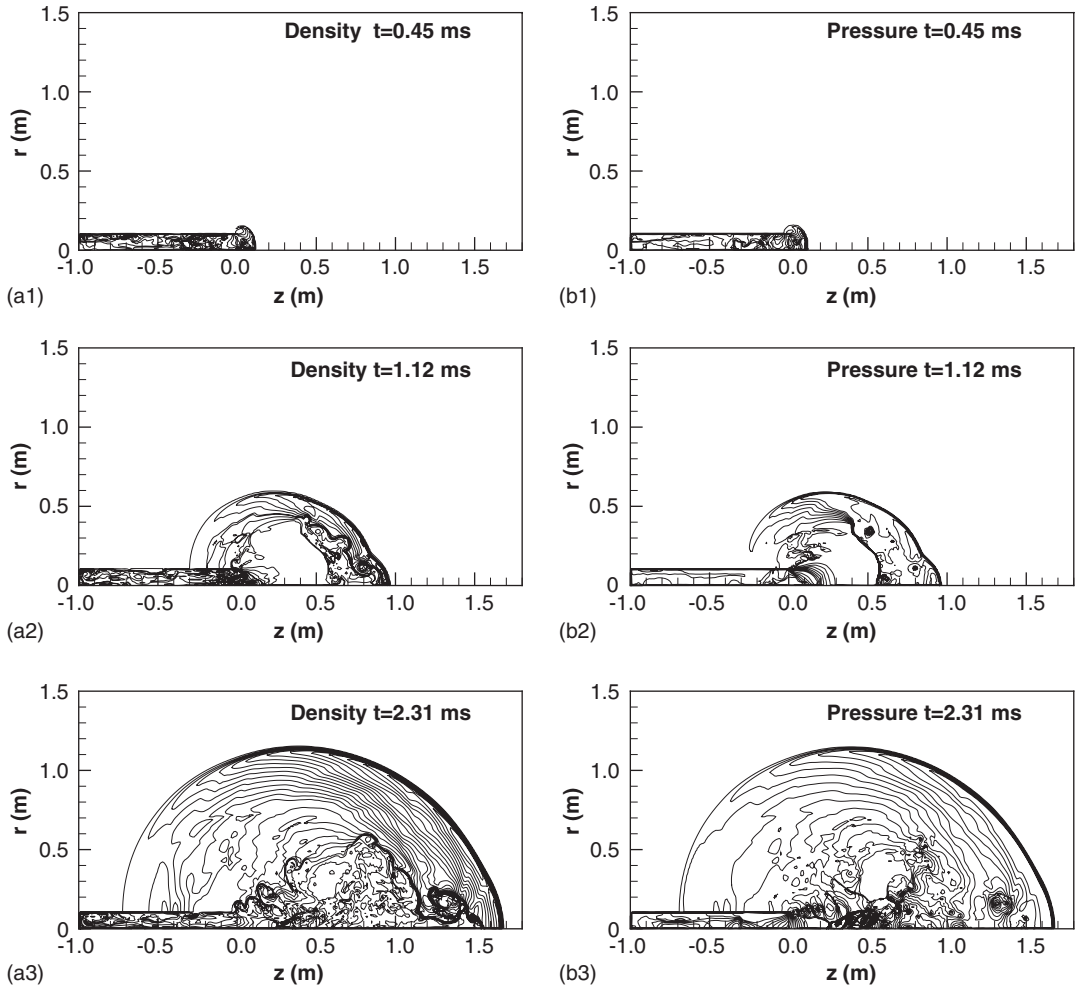

Figure 8. Blast wave propagation of two-dimensional simulation results at 0.45, 1.12 and 2.31 ms: (a1) density contours between 1.0 and 10.0 kg/m^3 in every 1.0 kg/m^3; (b1) pressure contours between 0.5 and 3.5 MPa in every 0.5 MPa; (a2) density contours between 0.5 and 4.0 kg/m^3 in every 0.25 kg/m^3; (b2) pressure contours between 0.6 and 8.0 MPa in every 0.2 MPa; (a3) density contours between 0.1 and 2.0 kg/m^3 in every 0.05 kg/m^3; and (b3) pressure contours between 0.4 and 2.0 MPa in every 0.1 MPa.

6.2. Three-dimensional simulation for the blast wave propagation around the magazine driven by the 32 kg TNT explosion in Cartesian coordinate

The three-dimensional blast wave simulation is performed on the same condition with the open-air mock experiment of the 32 kg TNT explosion of the underground magazine which was done in the exercises field of Japan Ground Self Defense Force in 2003 [36]. The heap with an earth was constructed and the magazine was horizontally embedded. The pyramid

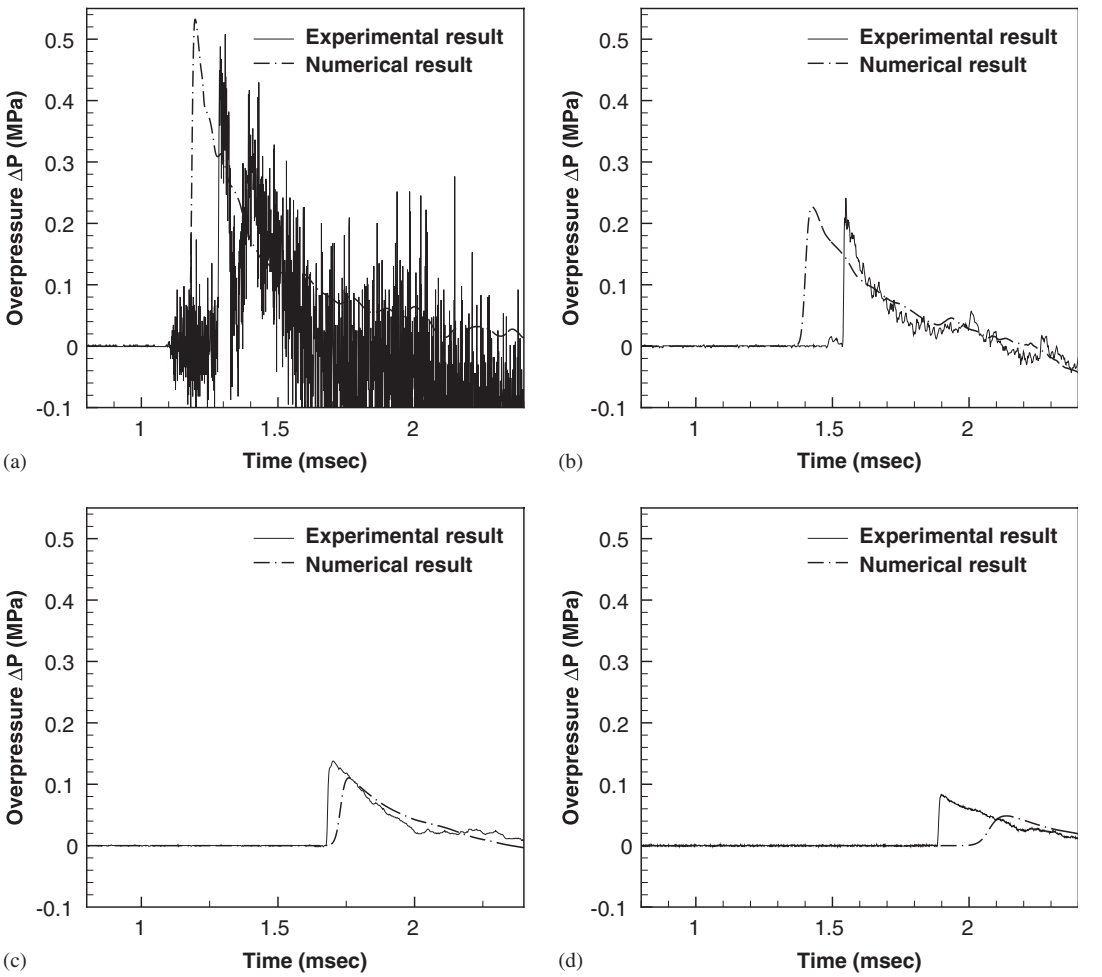

Figure 9. Overpressure history of two-dimensional simulation results at measurement points (dashed line) in comparison with experimental results (solid line): (a) $\theta = 1.8°$; (b) $\theta = 28°$; (c) $\theta = 60°$; and (d) $\theta = 85°$.

shape has the base area of $10\,\mathrm{m} \times 10\,\mathrm{m}$ and the height of 4.4 m and the magazine size is 5.0 m in length and 1.8 m in diameter. In the experiment, the peaks of the pressure history were measured at the several points on the ground with the distance of 22 and 36 m from the magazine outlet in various directions taking the angles of $0, 60, 120$ and $160°$ from the z-axis. The schematic of them is shown in Figure 10(a).

We set the x–z plane on the ground and the y-axis in the vertical direction and the origin of the coordinate system is located at the magazine outlet. It is assumed that the phenomena are symmetric due to the symmetric geometries of all the objects, so that we calculate only a half of the computational domain in the x direction. The grid number of $N_x \times N_y \times N_z = 180 \times 180 \times 450$ is assigned to the domain $0\,\mathrm{m} \leqslant x \leqslant 40\,\mathrm{m}$, $-20\,\mathrm{m} \leqslant z \leqslant 45\,\mathrm{m}$,

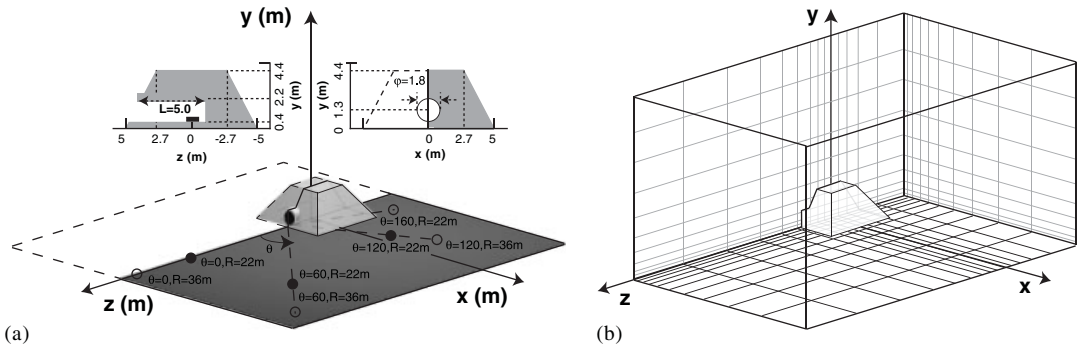

Figure 10. Computational domain of three-dimensional Cartesian coordinate: (a) a schematic of magazine with measurement points; and (b) a schematic of non-uniform Cartesian grid covering the computational domain.

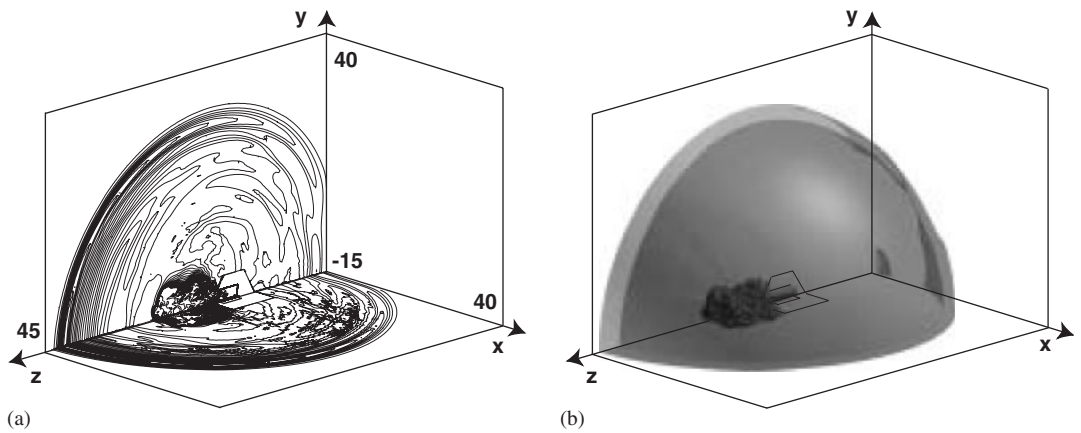

Figure 11. Blast wave propagation of three-dimensional simulation results at $t = 51.28$ ms: (a) contour plots of the density on the z–x and the z–y plane in the range of 0.5–1.35 kg/m^3 in every 0.01 kg/m^3; and (b) iso-surface plot of the volume fraction of 0.1 and the pressure of 1.05×10^5 Pa in the range of 63.2–115.6 kPa.

$0\,\mathrm{m} \leqslant y \leqslant 60\,\mathrm{m}$ in the Cartesian grid with non-uniform intervals. The fine meshes of $\Delta x = \Delta y = \Delta z = 0.1\,\mathrm{m}$ are arranged inside the magazine and around the outlet, and the distant meshes have larger size to $\Delta x = \Delta y = \Delta z = 0.4\,\mathrm{m}$ as shown in Figure 10(b).

The simulation was executed on the PC-Cluster of Intel Xeon 2.2 GHz $\times$ 40 with Myrinet2000 interconnection at Research Centre for Explosion Safety, National Institute of Advanced Industrial Science and Technology (AIST). It makes parallel computation possible that our numerical scheme is easily implemented to domain decomposition. The mesh resolution of $\Delta x = \Delta y = \Delta z = 0.1\,\mathrm{m}$ inside the magazine is too large for the size of 32 kg TNT, so that we calculate the propagation of the blast wave by using two-dimensional cylindrical simulation. When the front of the blast wave reaches the outlet, the two-dimensional result is

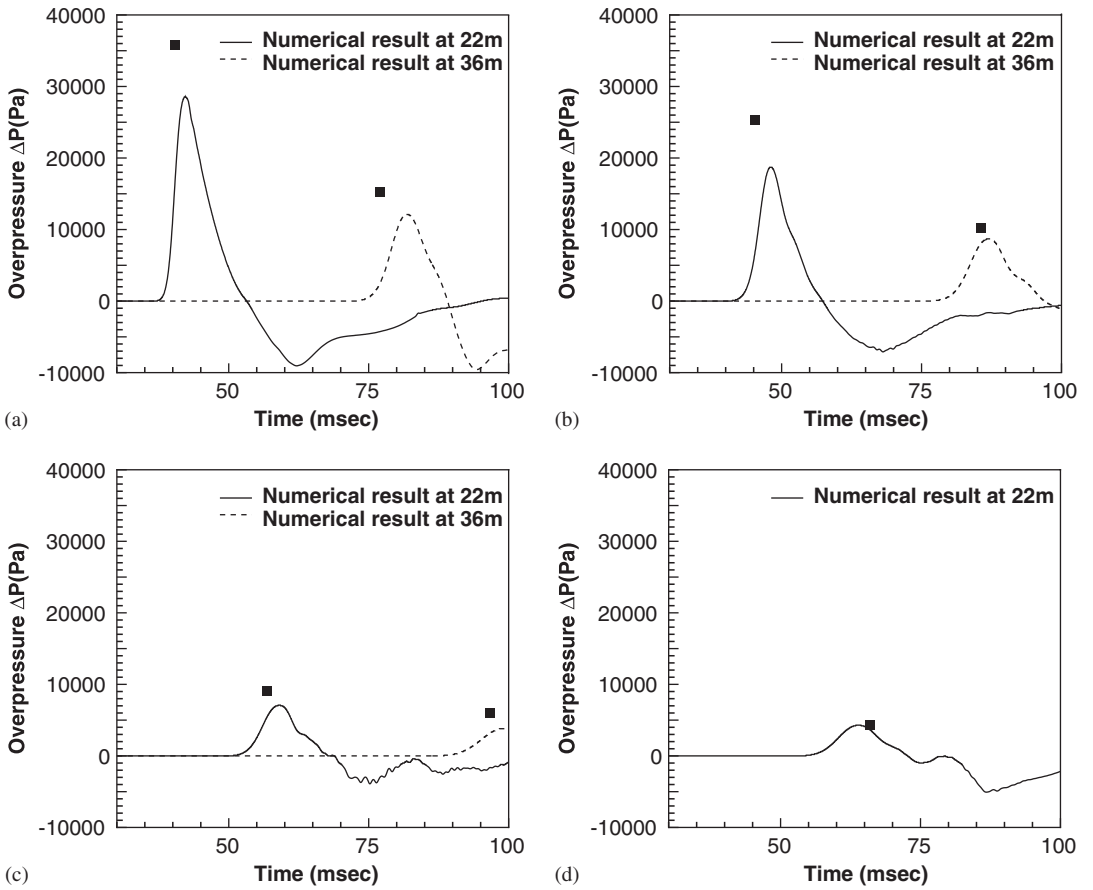

Figure 12. Overpressure history of three-dimensional simulation results at measurement points (solid lines and dashed lines) in comparison with experimental results (square symbols): (a) $\theta = 0^\circ$; (b) $\theta = 60^\circ$; (c) $\theta = 120^\circ$; and (d) $\theta = 160^\circ$.

planted in the three-dimensional Cartesian grid as the initial condition. The region outside the heap is filled with the air of the same parameters in the previous section. The rigid bodies are assumed for the heap with the magazine and the ground. The three-dimensional code is run with the CFL number of 0.2 and the artificial viscosity coefficient C_L of 2.0.

The density contour and the pressure iso-surface of the simulation result at the time of 51.28 ms are displayed in Figure 11(a) and (b). Almost spherical shock wave is described also in the three-dimensional simulation and it is qualitatively understood that the shock is stronger in the forward direction. The distribution of the detonation product gas is found in front of the magazine outlet and the interface to the air evolves unstably.

Figure 12 shows the history of the overpressure of the numerical results in comparison with the experimental data indicated by the square marks.

The same feature with the two-dimensional simulation is that the primary shock has the strongest pressure in the axial direction. It is found that the peaks and the arrival times of the shock is coincident with the experiment within 25% errors. In spite of large distances

from the outlet, the errors are seems to be quite small. In such far distance, the primary shock wave is followed by the rarefaction wave and the overpressures decrease to negative in time. In the three-dimensional simulation, the geometrical shape of the heap is accurately taken into consideration and unstable behaviour of the detonation product gas is different from two-dimensional simulation.

We discuss the mesh size and the computational domain size of the three-dimensional simulation from the view point of the scaling law. There is a similarity for the strength of blast wave with the scaling of $M^{-1/3}$, where M is the mass of the explosives. The mesh size of $\Delta x = 0.4\,\mathrm{m}$ for 32 kg TNT is normalized to 1 kg TNT and reduced to $0.031\,\mathrm{m/kg^{1/3}}$. The scaled distance of 40 m corresponds to $12\,\mathrm{m/kg^{1/3}}$. In the previous two-dimensional simulation with 0.1 kg pentolite, the mesh size of 0.0025 m is scaled to $0.0054\,\mathrm{m/kg^{1/3}}$ and the computation domain is reduced to $2\,\mathrm{m/kg^{1/3}}$. It is understood that the two-dimensional simulation uses about 1/6 times finer mesh for a smaller computational domain than those of the three-dimensional simulation, and gives us the better result.

7. CONCLUSIONS

For the simulation of strong blast waves, a high-accurate numerical scheme was presented. We introduce not only the values of the density, the velocity and the internal energy but also the special gradients of them as dependent variables. The fractional step procedure splits the compressible fluid equation into the advection phase and non-advection phase. The monotone preserving RCIP scheme is used for the density and the internal energy in the advection phase to avoid negative values, and the IDO scheme is adapted with three-stage Runge–Kutta time integration in the non-advection phase to describe the sound wave accurately. It is noticed that in both the phases, the schemes are based on the cubic Hermite interpolations constructed by the value and the gradient, and the overall numerical accuracy of the scheme keeps third order in space.

The applicability of the scheme to severe conditions is checked by the one-dimensional shock tube problem with the initial density and pressure jumps of thousands between left- and right-hand side. We also examine a well-known benchmark test for a long-distance propagation of the spherical shock driven by the free explosion from the local energy source. Both the results show enough good agreements with the analytic solution and the experimental data. Two- and three-dimensional simulations are performed for the blast waves driven by the explosion in the underground magazine. It is found that the numerical results successfully reproduce the pressure history measured at the several monitoring points on the ground.

It is concluded that the scheme proposed in this paper is quite available to solve the compressible fluid equation and applicable to the simulation of strong blast waves. Possible damage estimations of the blast wave will be given by the simulation based on our numerical scheme.

ACKNOWLEDGEMENTS

The authors thank the experimental group of Research Center for Explosion Safety in National Institute of Advanced Industrial Science and Technology (AIST) for giving the data of the explosion experiments and Dr T. Saburi for his help of computer operation. This work was supported by Grant-in-Aid

for Scientific Research from Japan Society for the Promotion of Science (B)(2) No. 16360045. The simulations were done on the Titech Grid System of GSIC, Tokyo Institute of Technology and the Bakoo PC Cluster of Research Center for Explosion Safety, AIST.

REFERENCES

1. Boris JP, Book DL. Flux-corrected transport. I. SHASTA, a fluid transport algorithm that works. *Journal of Computer Physics* 1973; **11**:38–69.
2. Roe PL. Approximate Riemann solvers, parameter vectors and difference schemes. *Journal of Computer Physics* 1981; **43**:357–372.
3. Osher S, Chakravarthy S. High resolution schemes and the entropy condition. *SIAM Journal on Numerical Analysis* 1984; **21**:955–984.
4. Harten A. High resolution schemes for hyperbolic conservation laws. *Journal of Computer Physics* 1983; **49**:357–393.
5. Yang H. An artificial compression method for ENO schemes: the slope modification method. *Journal of Computer Physics* 1990; **89**:125–160.
6. Harten A, Engquist B, Osher S, Chakravarthy SR. Uniformly high order accurate essentially non-oscillatory schemes, III. *Journal of Computer Physics* 1987; **71**:231–303.
7. Harten A. ENO schemes with subcell resolution. *Journal of Computer Physics* 1987; **83**:148–184.
8. Shu CW, Oshert S. Efficient implementation of essentially non-oscillatory shock-capturing schemes, II. *Journal of Computer Physics* 1989; **83**:32–78.
9. Woodward P, Colella P. The numerical simulation of two-dimensional fluid flow with strong shocks. *Journal of Computer Physics* 1984; **54**:115–173.
10. Colella P, Woodward PR. The piecewise parabolic method (PPM) for gas-dynamical simulations. *Journal of Computer Physics* 1984; **54**:174–201.
11. Brode HL. Numerical solution of spherical blast waves. *Journal of Applied Physics* 1955; **26**:766–775.
12. Brode HL. Blast wave from a spherical charge. *Physics of Fluids* 1959; **2**:217–229.
13. Kury JW, Hornig HC, Lee EL, McDonnel JW, Ornellas DL, Finger M, Starnge FM, Wilkins ML. Metal acceleration by chemical explosives. *Fourth Symposium on Detonation* 1965; 3–13.
14. Jones DL. Blast waves and scaling laws. *Physics of Fluids* 1970; **13**:1398–1399.
15. Ofengeim DKh, Drikakis D. Simulation of blast wave propagation over a cylinder. *Shock Waves* 1997; **7**:305–317.
16. Cieslak S, Ben Khelil S, Choquet I, Merlen A. Cut cell strategy for 3-D blast waves numerical simulations. *Shock Waves* 2001; **10**:241–249.
17. Liang SM, Wang JS, Chen H. Numerical study of spherical blast-wave propagation and reflection. *Shock Waves* 2002; **12**:59–68.
18. Dobratz BM. *Properties of Chemical Explosives and Explosive Simulants*. LLNL Explosives Handbook UCRL-52997 Distribution Category UC-45.
19. Mader CL. Shock and hot spot initiation of homogeneous explosives. *Physics of Fluids* 1963; **6**:375–381.
20. Yu Vorobiev O, Lomov IN. Numerical simulation of gas–solid interface with large deformations. *International Conference on Computational Engineering Science*, Los Angeles, CA, vol. 1. Tech Science Press, 2000; 922–927.
21. Yabe T, Aoki T. A universal solver for hyperbolic equations by cubic-polynomial interpolation I. One-dimensional solver. *Computer Physics Communications* 1991; **66**:219–232.
22. Yabe T, Xiao F, Utsumi T. Constrained interpolation profile method for multiphase analysis. *Journal of Computer Physics* 2001; **169**:556–593.
23. Xiao F, Yabe T, Ito T. Constructing oscillation preventing scheme for advection equation by rational function. *Computer Physics Communications* 1996; **93**(1):1–12.
24. Xiao F, Yabe T, Nizam G, Ito T. Constructing a multi-dimensional oscillation preventing scheme for the advection equation by a rational function. *Computer Physics Communications* 1996; **94**(2–3):103–118.
25. Aoki T. Interpolated differential operator (IDO) scheme for solving partial differential equations. *Computer Physics Communications* 1997; **102**(1–3):132–146.
26. Yoshida H, Aoki T, Utsumi T. Improvement of accuracy and stability in numerical solving hyperbolic equations by IDO (Interpolated Differential Operator) scheme with Runge–Kutta time integration. *Fundamentals of Electronics, Communications and Computer Sciences* 2003; **J86-A**:223–231.
27. Wilkins ML. Use of artificial viscosity in multidimensional fluid dynamic calculations. *Journal of Computational Physics* 1980; **36**:281–303.
28. Aoki T. Multi-dimensional advection of CIP (Cubic Interpolated Propagation) scheme. *Computer Fluid Dynamics Journal* 1995; **4**:279–291.

29. Yabe T, Mizoe H, Takizawa K, Moriki H, Im HN, Ogata Y. Higher-order schemes with CIP method and adaptive soroban grid towards mesh-free scheme. *Journal of Computational Physics* 2004; **194**:57–77.
30. Baker WE. *Explosions in Air*. University of Texas Press: Austin, 1973; 150.
31. Sedov LI. *Similarity and Dimensional Methods in Mechanics*. Academic Press: New York, 1959.
32. Taylor GI. The formulation of blast wave by a very intense explosion. *Proceedings of the Royal Society of London*, *Series A* 1950; 159–186.
33. von Neumann J. *Blast Waves*. Los Alamos Science Laboratory, Technical Series, 1947.
34. Zel'dovich YB, Raizer YuP. *Physics of Shock Waves and High-Temperature Hydro-dynamic Phenomena*. Academic Press: New York, 1966.
35. Nakayama Y, Matsumura T, Miyamoto K, Iida M, Yoshida M. *Kayaku Gakkaishi* 1999; **60**:293.
36. *Bakuhatsu-eikyou-hyouka-iinkai-houkoku-sho*. All Japan Association for Security of Explosives, 2003.

